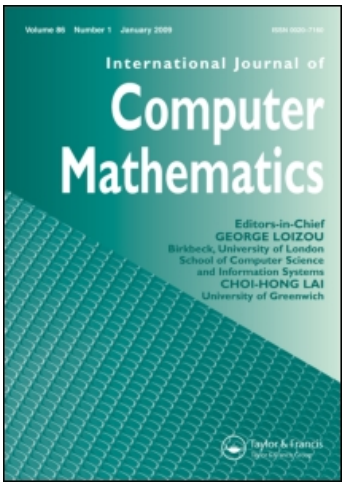

International Journal of Computer Mathematics
Publication details, including instructions for authors and subscription information:
http://www.informaworld.com/smpp/title~content=t713455451

Torus bifurcations, isolas and chaotic attractors in a simple dengue fever model with ADE and temporary cross immunity

Maíra Aguiar [ab]; Nico Stollenwerk [ab]; Bob W. Kooi [c]
[a] Centro de Matemática e Aplicações Fundamentais, Universidade de Lisboa, Lisboa, Portugal [b] Instituto Gulbenkian de Ciência, Oeiras, Portugal [c] Faculty of Earth and Life Sciences, Department of Theoretical Biology, Vrije Universiteit Amsterdam, Amsterdam, The Netherlands

Online Publication Date: 01 October 2009

To cite this Article Aguiar, Maíra, Stollenwerk, Nico and Kooi, Bob W.(2009)'Torus bifurcations, isolas and chaotic attractors in a simple dengue fever model with ADE and temporary cross immunity',International Journal of Computer Mathematics,86:10,1867 — 1877
To link to this Article: DOI: 10.1080/00207160902783532
URL: http://dx.doi.org/10.1080/00207160902783532

International Journal of Computer Mathematics
Vol. 86, Nos. 10–11, October–November 2009, 1867–1877

Taylor & Francis
Taylor & Francis Group

Torus bifurcations, isolas and chaotic attractors in a simple dengue fever model with ADE and temporary cross immunity

Maíra Aguiar[a,b]*, Nico Stollenwerk[a,b] and Bob W. Kooi[c]

[a] *Centro de Matemática e Aplicações Fundamentais, Universidade de Lisboa, Avenida Prof. Gama Pinto 2, 1649-003 Lisboa, Portugal;* [b] *Instituto Gulbenkian de Ciência, Apartado 14, 2781-901 Oeiras, Portugal;* [c] *Faculty of Earth and Life Sciences, Department of Theoretical Biology, Vrije Universiteit Amsterdam, De Boelelaan 1087, NL 1081 HV Amsterdam, The Netherlands*

(*Received 30 July 2008; final version received 27 January 2009*)

We analyse an epidemiological model of competing strains of pathogens and hence differences in transmission for first versus secondary infection due to interaction of the strains with previously aquired immunities, as has been described for dengue fever, is known as antibody dependent enhancement (ADE). These models show a rich variety of dynamics through bifurcations up to deterministic chaos. Including temporary cross-immunity even enlarges the parameter range of such chaotic attractors, and also gives rise to various coexisting attractors, which are difficult to identify by standard numerical bifurcation programs using continuation methods. A combination of techniques, including classical bifurcation plots and Lyapunov exponent spectra, has to be applied in comparison to get further insight into such dynamical structures. Here we present for the first time multi-parameter studies in a range of biologically plausible values for dengue. The multi-strain interaction with the immune system is expected to have implications for the epidemiology of other diseases also.

Keywords: numerical bifurcation analysis; Lyapunov exponents; $\mathbb{Z}_2$ symmetry; epidemiology; antibody dependent enhancement (ADE)

2000 AMS Subject Classifications: 34C23; 37G35; 37G40; 37D45; 65P30; 92B05

1. Introduction

Epidemic models are classically phrased in ordinary differential equation (ODE) systems for the host population divided into classes of susceptible individuals and infected ones (SIS system), or in addition, a class of recovered individuals owing to immunity after an infection to the respective pathogen (SIR epidemics). The infection term includes a product of two variables, hence a nonlinearity which in extended systems can cause complicated dynamics. Although these simple SIS and SIR models only show equilibria as stationary solutions, they already show non-trivial equilibria arising from bifurcations, and in stochastic versions of the system critical fluctuations at the critical point. Further refinements of the SIR model in terms of external forcing or distinction of infections with different strains of a pathogen, hence classes of (a) individuals infected with one or

*Corresponding author. Email: maira@ptmat.fc.ul.pt

ISSN 0020-7160 print/ISSN 1029-0265 online

DOI: 10.1080/00207160902783532
http://www.informaworld.com

another strain, (b) those recovered from the infection by one or another strain, (c) those infected with more than one strain, etc. can induce more complicated dynamical attractors, including equilibria, limit cycles, tori and chaotic attractors.

Classical examples of chaos in epidemiological models are provided by childhood diseases with extremely high infection rates, so that a moderate seasonal forcing can generate Feigenbaum sequences of period doubling bifurcations into chaos. Success in analysing childhood diseases in terms of modelling and data comparison lies in the fact that they are just childhood diseases with such high infectivity. Otherwise host populations cannot sustain the respective pathogens. In other infectious diseases much lower forces of infection have to be considered leading to further conceptual problems with noise affecting the system more than the deterministic part do. This shows even critical fluctuations with power law behaviour, when considering evolutionary processes of harmless strains of pathogens versus occasional accidents of pathogenic mutants [21]. In these circumstances only explicitly stochastic models, of which the classical ODE models are mean field versions, can capture the fluctuations observed in time series data [22].

The situation is again different in multi-strain models, which have attracted attention recently. It has been demonstrated that the interaction of various strains on the infection of the host with eventual cross-immunities or other interactions between host immune system and multiple strains can generate complicated dynamic attractors. A prime example is dengue fever. A first infection is often mild or even asymptomatic and leads to life long immunity against this strain. However, a subsequent infection with another strain of the virus often causes clinical complications up to life threatening conditions and hospitalization, owing to ADE. More on the biology of dengue and its consequences for the detailed epidemiological model structure can be found in Aguiar and Stollenwerk [1], including literature on previous modelling attempts. For additional literature on dengue models see also [16]. On the biological evidence for ADE see e.g. [12]. In addition to the difference in the force of infection between primary and secondary infection, parametrized by a so-called ADE parameter ϕ, which has been demonstrated to show chaotic attractors in a certain parameter region, namley only for very high contribution of secondary infected to the force of infection, another effect, the temporary cross-immunity after a first infection against all dengue virus strains, parametrized by the temporary cross-immunity rate α, shows bifurcations up to chaotic attractors in a much wider and biologically more realistic parameter region, even for lowered contribution of secondary infected to the force of infection. Biologically, secondary infected hosts develop severe symptoms much more often than first infected and hence are then hospitalized, which means they contribute less likely to the force of infection [1].

The model presented in the appendix has been described in detail in [1] and has recently been analysed for a parameter value of $\alpha = 2\,\text{year}^{-1}$ corresponding on average to half a year of biologically plausible temporary cross immunity [2]. At low ADE parameter ϕ there is a stable equilibrium. When increasing ϕ, this equilibrium bifurcates via a Hopf bifurcation into a stable limit cycle and then after further continuation the limit cycle becomes unstable in a torus bifurcation. This torus bifurcation can be located using numerical bifurcation software based on continuation methods tracking known equilibria or limit cycles up to bifurcation points [7]. The continuation techniques and the theory behind it are described, e.g. in Kuznetsov [15].

Complementary methods like Lyapunov exponent spectra can also characterize chaotic attractor [18,20], and lead eventually to the detection of coexisting attractors to the main limit cycles and tori originated from the analytically accessible equilibrium for small ϕ. Such coexisting structures are often missed in bifurcation analysis of higher dimensional dynamical systems but are demonstrated to be crucial at times in understanding qualitatively the real world data, as for example demonstrated previously in a childhood disease study [8]. In such a study first the understanding of the deterministic system's attractor structure is needed, and then eventually the interplay between attractors mediated by population noise in the stochastic version of the system gives the full understanding of the data.

Here we present for the first time extended results of the bifurcation structure for various parameter values of the temporary cross immunity α in the region of biological relevance and multi-parameter bifurcation analysis. In addition to the torus bifurcation route to chaos, this also reveals the classical Feigenbaum period doubling sequence and the origin of the so-called isola solutions.

The different strains of the dengue fever virus are genetically and antigenically very similar, and therefore cause the confusion in the immune response known as ADE [1]. Hence for the host the different strains look similar, leading to identical parameters in dengue models for the different strains, which causes symmetry in the model system. This symmetry of the different strains leads to symmerty breaking bifurcations of limit cycles, which are rarely described in the epidemiological literature but well known in the biochemical literature, e.g. for coupled identical cells. The interplay between different numerical procedures and basic analytic insight in terms of symmetries help to understand the attractor structure of multi-strain interactions in the present case of dengue fever, and will contribute to the final understanding of dengue epidemiology including the observed fluctuations in real world data. In the literature the multi-strain interaction leading to deterministic chaos via ADE has been described previously, e.g. [4,10], but neglecting temporary cross immunity and hence getting stuck in rather biologically unrealistic parameter regions, whereas more recently the considerations of temporary cross immunity in rather complicated and up to now models, which are not analysed in great detail but include all kinds of interations, have appeared for the first time [17,24], in this case failing to investigate the possible dynamical structures in more detail.

2. Dynamical system

The multistrain model under investigation can be given as an ODE system

$$\frac{\mathrm{d}}{\mathrm{d}t}\underline{x} = \underline{f}(\underline{x}, \underline{a}) \tag{1}$$

for the state vector of the epidemiological host classes $\underline{x} := (S, I_1, I_2, \ldots, R)^{\mathrm{tr}}$ and besides other fixed parameters which are biologically undisputed the parameter vector of varied parameters $\underline{a} = (\alpha, \phi)^{\mathrm{tr}}$, with tr for transpose of a vector or a matrix. For a detailed description of the biological content of state variables and parameters see [1]. The ODE equations and fixed parameter values are given in the appendix. The equilibrium values $\underline{x}^*$ are given by the equilibrium condition $\underline{f}(\underline{x}^*, \underline{a}) = 0$, respectively, for limit cycles $\underline{x}^*(t + T) = \underline{x}^*(t)$ with period T. For chaotic attractors the trajectory of the dynamical system reaches in the time limit of infinity the attractor trajectory $\underline{x}^*(t)$, equally for tori with irrational winding ratios. In all cases the stability can be analysed considering small perturbations $\Delta\underline{x}(t)$ around the attractor trajectories

$$\frac{\mathrm{d}}{\mathrm{d}t}\Delta\underline{x} = \left.\frac{\mathrm{d}\underline{f}}{\mathrm{d}\underline{x}}\right|_{\underline{x}^*(t)} \cdot \Delta\underline{x}. \tag{2}$$

Here, any attractor is notified by $\underline{x}^*(t)$, be it an equilibrium, periodic orbit or chaotic attractor. In this ODE system the linearized dynamics is given with the Jacobian matrix $(\mathrm{d}\underline{f}/\mathrm{d}\underline{x})$ of the ODE system equation (1) evaluated at the trajectory points $\underline{x}^*(t)$ given in notation of $(\mathrm{d}\underline{f}/\mathrm{d}\underline{x})|_{\underline{x}^*(t)}$. The Jacobian matrix is analysed for equilibria in terms of eigenvalues to determine stability and the loss of it at bifurcation points, negative real part indicating stability. For the stability and loss of it for limit cylces Floquet multipliers are more common (essentially the exponentials of eigenvalues), multipliers inside the unit circle indicating stability, and where they leave eventually the unit circle determining the type of limit cycle bifurcations. And for chaotic systems Lyapunov

exponents are determined from the Jacobian around the trajectory, positive largest exponents showing deterministic chaos, zero largest showing limit cycles including tori, largest smaller zero indicating fixed points.

2.1 *Symmetries*

To investigate the bifurcation structure of the system under investigation we first observe the symmetries due to the multi-strain structure of the model.

These symmetries reflect the similarities of the different strain for the host specific properties modelled here, namely the social contact rate and infectivity and the immune response [1]. The observation of symmetries due to the multi-strain structure becomes important for the time being for equilibria[1] and limit cycles. We introduce the following notation: With a symmetry transformation matrix **S**

$$\mathbf{S} := \begin{pmatrix} 1 & 0 & 0 & 0 & 0 & 0 & 0 & 0 & 0 & 0 \\ 0 & 0 & 1 & 0 & 0 & 0 & 0 & 0 & 0 & 0 \\ 0 & 1 & 0 & 0 & 0 & 0 & 0 & 0 & 0 & 0 \\ 0 & 0 & 0 & 0 & 1 & 0 & 0 & 0 & 0 & 0 \\ 0 & 0 & 0 & 1 & 0 & 0 & 0 & 0 & 0 & 0 \\ 0 & 0 & 0 & 0 & 0 & 0 & 1 & 0 & 0 & 0 \\ 0 & 0 & 0 & 0 & 0 & 1 & 0 & 0 & 0 & 0 \\ 0 & 0 & 0 & 0 & 0 & 0 & 0 & 0 & 1 & 0 \\ 0 & 0 & 0 & 0 & 0 & 0 & 0 & 1 & 0 & 0 \\ 0 & 0 & 0 & 0 & 0 & 0 & 0 & 0 & 0 & 1 \end{pmatrix} \tag{3}$$

we have the following symmetry:

If

$$\underline{x}^* = \left(S^*, I_1^*, I_2^*, R_1^*, R_2^*, S_1^*, S_2^*, I_{12}^*, I_{21}^*, R^*\right)^{\mathrm{tr}} \tag{4}$$

is equilibrium or limit cycle, then also

$$\mathbf{S}\underline{x}^* = \left(S^*, I_2^*, I_1^*, R_2^*, R_1^*, S_2^*, S_1^*, I_{21}^*, I_{12}^*, R^*\right)^{\mathrm{tr}} \tag{5}$$

with $\underline{x}^*$ equilibrium values or $\underline{x}^* = \underline{x}^*(t)$ limit cycle for all times $t \in [0, T]$. For the right-hand side $\underline{f}$ of the ODE system equation (1) the kind of symmetry found above is called $\mathbb{Z}_2$-symmetry when the following equivariance condition holds:

$$\underline{f}(\mathbf{S}\underline{x}, \underline{a}) = \mathbf{S}\underline{f}(\underline{x}, \underline{a}) \tag{6}$$

with **S** a matrix that obeys $\mathbf{S} \neq \mathbf{I}$ and $\mathbf{S}^2 = \mathbf{I}$, where **I** is the unit matrix. Observe that besides **S I** also satisfies Equation (6). The symmetry transformation matrix **S** in Equation (3) fulfills these requirements. It is easy to verify that the $\mathbb{Z}_2$-equivariance conditions in Equation (6) and the properties of **S** are satisfied for our ODE system. In Seydel [23] a simplified version of the famous Brusselator that shows this type of symmetry is discussed. There, an equilibrium and also a limit cycle show a pitchfork bifurcation with symmetry breaking.

An equilibrium $\underline{x}^*$ is called *fixed* when $\mathbf{S}\underline{x}^* = \underline{x}^*$ (see [15]). Two equilibria $\underline{x}^*, \underline{y}^*$ where $\mathbf{S}\underline{x}^* \neq \underline{x}^*$, are called **S**-conjugate if their corresponding solutions satisfy $\underline{y}^* = \mathbf{S}\underline{x}^*$ (and because $\mathbf{S}^2 = \mathbf{I}$ also $\underline{x}^* = \mathbf{S}\underline{y}^*$). For limit cycles a similar terminology is introduced. A periodic solution is called *fixed* when $\mathbf{S}\underline{x}^*(t) = \underline{x}^*(t)$ and the associated limit cycles are also called *fixed* [15].

There is another type of periodic solution that is not fixed but called *symmetric* when

$$\mathbf{S}\underline{x}^*(t) = \underline{x}^*\left(t + \frac{T}{2}\right), \tag{7}$$

where T is the period. Again the associated limit cycles are also called *symmetric*. Both types of limit cycles L are **S**-invariant as curves: $\mathbf{S}L = L$. That is, in the phase-plane where time parameterizes the orbit, the cycle and the transformed cycle are equal. A **S**-invariant cycle is either fixed or symmetric. Two noninvariant limit cycles ($\mathbf{S}L \neq L$) are called **S**-conjugate if their corresponding periodic solutions satisfy $\underline{y}^*(t) = \mathbf{S}\underline{x}^*(t), \forall t \in \mathbb{R}$. The properties of the symmetric systems and the introduced terminology are used below with the interpretation of the numerical bifurcation analysis results. We refer to [15] for an overview of the possible bifurcations of equilibria and limit cycles of $\mathbb{Z}_2$-equivariant systems.

3. Bifurcation diagrams for various α values

We show the results of the bifurcation analysis in bifurcation diagrams for several α values, varying ϕ continuously. In addition to the previously investigated case of $\alpha = 2\,\text{year}^{-1}$, we show also a case of smaller and a case of larger α value, obtaining more information on the bifurcations possible in the model as a whole. The above-mentioned symmetries help in understanding the present bifurcation structure.

3.1 *Bifurcation diagram for $\alpha = 3$*

For $\alpha = 3$ the one-parameter bifurcation diagram is shown in Figure 1(a). Starting with $\phi = 0$ there is a stable fixed equilibrium, fixed in the above-mentioned notion for symmetric systems. This equilibrium becomes unstable at a Hopf bifurcation H at $\phi = 0.16445$. A stable fixed limit cycle originates at this Hopf bifurcation. This limit cycle shows a supercritical pitch-fork bifurcation P^-, i.e. a bifurcation of a limit cycle with Floquet multiplier 1, splitting the original limit cycle into two new ones. In addition to the now unstable branch two new branches originate for the pair of conjugated limit cycles. The branches merge again at another supercritical pitch-fork bifurcation

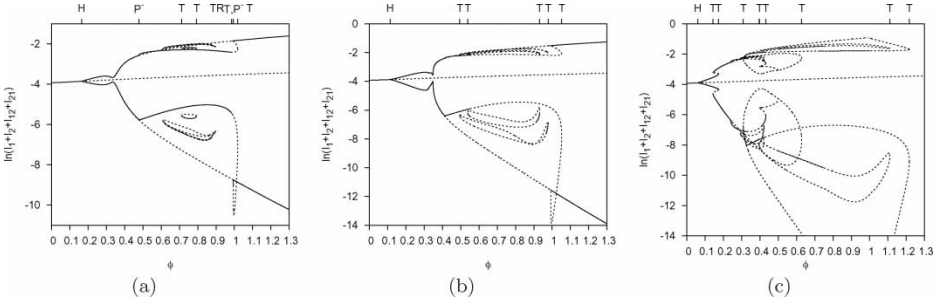

Figure 1. (a) $\alpha = 3$. Equilibria or extremum values for limit cycles for logarithm of total infected $I_1 + I_2 + I_{12} + I_{21}$. Solid lines denote stable equilibria or limit cycles, dashed lines unstable equilibria or periodic-one limit cycles. Hopf bifurcation H around $\phi = 0.16$ two pitchfork bifurcations P^- and a torus bifurcation TR. In addition to this main bifurcation structure we found coexisting tangent bifurcations T between which some of the isolas live, see especially the one between $\phi = 0.71$ and 0.79. Additionally found flip bifurcations are not marked here, see text. (b) $\alpha = 2$. In this case we have a Hopf bifurcation H at $\phi = 0.11$, and besides the similar structure found in (a) also more separated tangent bifurcations T exist at $\phi = 0.494$, 0.539, 0.931, 0.978 and 1.052, (c) $\alpha = 1$. Here we have the Hopf bifurcation at $\phi = 0.0598$ and thereafter many tangent bifurcations T, again with coexisting limit cylces.

P^-, after which the limit cycle is stable again for higher ϕ-values. The pair of **S**-conjugate limit cycles become unstable at a torus bifurcation TR at $\phi = 0.89539$.

In addition to this main bifurcation pattern we found two isolas, that is an isolated solution branch of limit cycles [11]. These isola cycles L are not **S**-invariant, that is $\mathbf{S}L \neq L$. Isolas consisting of isolated limit cycles exist between two tangent bifurcations. One isola consists of a stable and an unstable branch. The other one shows more complex bifurcation patterns. There is no fully stable branch. For $\phi = 0.60809$ at the tangent bifurcation T, a stable and an unstable limit cycle collide. The stable branch becomes unstable via a flip bifurcation or a periodic doubling bifurcation F, with Floquet multiplier (-1), at $\phi = 0.61918$, which is also a pitchfork bifurcation for the period-two limit cycles. At the other end of that branch at the tangent bifurcation T at $\phi = 0.89768$ both colliding limit cycles are unstable. Close to this point at one branch there is a torus bifurcation TR, also called Neimark–Sacker bifurcation, at $\phi = 0.89539$ and a flip bifurcation F at $\phi = 0.87897$, which is again a pitchfork bifurcation P for the period-two limit cycles. Continuation of the stable branch originating for the flip bifurcation F at $\phi = 0.61918$ gives another flip bifurcation F at $\phi = 0.62070$ and one close to the other end at $\phi = 0.87897$, namely at $\phi = 0.87734$. These results suggest that for this isola two classical routes to chaos can exist, namely via the torus or Neimark–Sacker bifurcation, where the dynamics on the originating torus is chaotic, and the cascade of period doubling route to chaos.

3.2 *Bifurcation diagram for* $\alpha = 2$

For $\alpha = 2$ the one-parameter bifurcation diagram is shown in Figure 1(b). The stable fixed equilibrium becomes unstable at a supercritical Hopf bifurcation H at $\phi = 0.11329$ where a stable fixed limit cycle originates. This stable limit cycle becomes unstable at a superciritcal pitchfork bifurcation point P^- at $\phi = 0.41145$ for a limit cycle. This point marks the origin of a pair of **S**-conjugate stable limit cycles apart from the now unstable fixed limit cycle. Here one has to consider the two infected subpopulations I_1 and I_2 to distinguish the conjugate limit cycles. The two variables I_1 and I_2 are being interchangeable, this can also be interpreted as the stable limit cycles for the single variable say I_1. The fixed stable equilibrium below the Hopf bifurcation where we have $I_1^* = I_2^*$, $R_1^* = R_2^*$, $S_1^* = S_2^*$ and $I_{12}^* = I_{21}^*$ is a fixed equilibrium. For the fixed limit cycle in the parameter interval between the Hopf bifurcation and the pitchfork bifurcation we have $I_1^*(t) = I_2^*(t)$, $R_1^*(t) = R_2^*(t)$, $S_1^*(t) = S_2^*(t)$ and $I_{12}^*(t) = I_{21}^*(t)$. This means that at the Hopf bifurcation H the stable fixed equilibrium becomes an unstable fixed equilibrium. In the parameter interval between the two pitchfork bifurcations P^- at $\phi = 0.41145$ and subcritical P^+ at $\phi = 0.99214$, two stable limit cycles coexist and these limit cycles are **S**-conjugate. At the pitchfork bifurcation points the fixed limit cycle becomes unstable and remains fixed, and two stable **S**-conjugate limit cycles originate (see [15, Theorem 7.7]). The invariant plane $I_1 = I_2$, $R_1 = R_2$, $S_1 = S_2$, $I_{12} = I_{21}$ forms the separatrix between the pair of stable **S**-conjugate limit cycles $x^*(t)$ and $\mathbf{S}x^*(t)$, $\forall t \in \mathbb{R}$. The initial values of the two state variables $S(t_0)$ and $R(t_0)$, together with the point on the invariant plane, determine to which limit cycle the system converges. Continuation of the stable symmetric limit cycle gives a torus or Neimark–Sacker bifurcation at the point denoted by TR at $\phi = 0.55069$. At this point the limit cycles become unstable because a pair of complex-conjugate multipliers crosses the unit circle. Observe that at this point in the time series plot [1, Figure 12] the chaotic region starts. In [3] the following route to chaos, namely the sequence of Neimark–Sacker bifurcations into chaos, is mentioned. Increasing the bifurcation parameter ϕ along the now unstable pair of **S**-conjugate limit cycles leads to a tangent bifurcation T at $\phi = 1.0524$, where a pair of two unstable limit cycles collide. This branch terminates at the second pitchfork bifurcation point denoted by P^+ at $\phi = 0.99214$. Since the first fold point gave rise to a stable limit cycle and this fold point to an unstable limit cycle, we call the first pitchfork

bifurcation *supercritical* and the latter pitchfork bifurcation *subcritical*. These results agree very well with the simulation results shown in the bifurcation diagram for the maxima and minima of the overall infected (see Figure 15 in [1]). Notice that AUTO [7] calculates only the global extrema during a cycle, not the local extrema. Figure 1(b) shows also two isolas similar to those for $\alpha = 3$ in Figure 1(a).

3.3 *Bifurcation diagram for* $\alpha = 1$

For $\alpha = 1$ the bifurcation diagram is shown in Fig. 1(c). In the lower ϕ parameter range there is bistability of two limit cycles in an interval bounded by two tangent bifurcations T. The stable manifold of the intermediate saddle limit cycle acts as a separatrix. Inceasing ϕ the stable limit cycles become unstable at the pitchfork bifurcation P at $\phi = 0.23907$. Following the unstable primary branch, for larger values of ϕ we observe an open loop bounded by two tangent bifurcations T. The extreme value for ϕ is at $\phi = 0.62790$. Then lowering ϕ there is a pitchfork bifurcation P at $\phi = 0.50161$. Later we will return to the description of this point. While lowering ϕ further the limit cycle becomes stable again at the tangent bifurcations T at $\phi = 0.30863$. On increasing ϕ this limit cycle becomes unstable again at the pitchfork bifurcation P at $\phi = 0.32532$.

Continuation of the secondary branch of the two **S**-conjugated limit cycles from this point reveals that the stable limit cycle becomes unstable at a torus bifurcation TR at $\phi = 0.42573$. The simulation results depicted in [1, Figure 13] show that there is chaos beyond this point. The secondary pair of **S**-conjugate limit cycles that originate from pitchfork bifurcation P at $\phi = 0.23907$ becomes unstable at a flip bifurcation F. Increasing ϕ further it becomes stable again at a flip bifurcation F. Below we return to the interval between these two flip bifurcations. The stable part becomes unstable at a tangent bifurcation T, then continuing, after a tangent bifurcation T and a Neimark–Sacker bifurcation TR. This bifurcation can lead to a sequence of Neimark–Sacker bifurcations into chaos. The unstable limit cycles terminates via a tangent bifurcation F where the primary limit cycle possesses a pitchfork bifurcation P at $\phi = 0.50161$. At the flip bifurcation F the cycle becomes unstable and a new stable limit cycle with double period emanates. The stable branch becomes unstable at a flip bifurcation again. We conclude that there is a cascade of period doubling route to chaos. Similarly this happens in reversed order ending at the flip bifurcation where the secondary branch becomes stable again.

Figure 2(a) gives the results for the interval $0.28 \leq \phi \leq 0.44$, where only the minima are shown. In this plot also a 'period three' limit cycle is shown. In a small region it is stable and coexists together with the 'period one' limit cycle. The cycles are shown in Figure 2(b) and (c) for $\phi = 0.294$. The one in Figure 2(c) looks like a period-3 limit cycle. In Figure 2 continuation

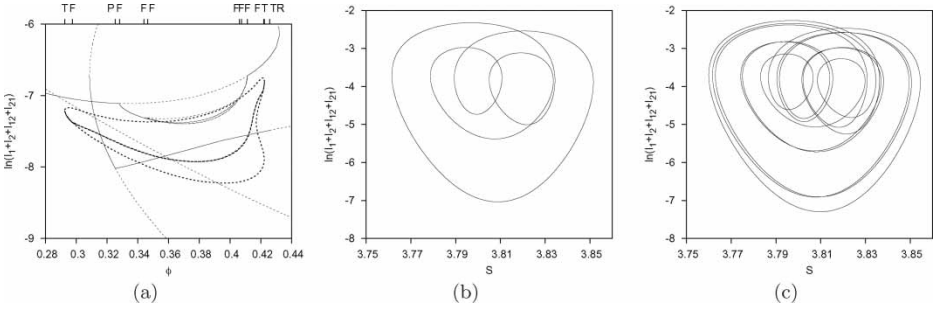

Figure 2. (a) $\alpha = 1$. Detail of Figure 1(c). We find pitchfork bifurcations P at $\phi = 0.239$ and 0.325, flip bifurcations F at $\phi = 0.298$, 0.328,0.344,0.346, 0.406, 0.407, 0.411 and 0.422, further tangent bifurcations T at $\phi = 0.292$, 0.346 and 0.422. Four almost coexisting bifurcations, namely F's at $\phi = 0.4112590$. (b) and (c) state space-plots of susceptibles and logarithm of infected for $\alpha = 1$ and $\phi = 0.294$ for two coexisting stable limit cycles.

of the limit cycle gives a closed graph bounded at the two ends by tangent bifurcations T, where a stable and an unstable limit cycles collide. The intervals where the limit cycle is stable, are on the other end bounded by flip bifurcations F. One unstable part intersects the higher period cycles that originate via the cascade of period doubling between the period-1 limit cycle flip bifurcations F at $\phi = 0.32816$ and 0.41126. This suggest that the period-3 limit cycle is associated with a 'period-3 window' of the chaotic attractor. We conjecture that this interval is bounded by two homoclinic bifurcations for a period-3 limit cycle [5,6,13,14]. The bifurcation diagram shown in [1, Figure 13] shows the point where the chaotic attractor disappears abruptly, possible at one of the two homoclinic bifurcations. In that region the two conjugated limit cycles that originate at the pitchfork bifurcation P at $\phi = 0.32532$ are the attractors. These results suggest that there are chaotic attractors associated with the period-1 limit cycle, one occurs via a cascade of flip bifurcations originating from the two ends at $\phi = 0.32816$ and $\phi = 0.41126$ and one via a Neimark–Sacker bifurcation TR at $\phi = 0.42573$.

4. Two-parameter diagram

We will now link the three studies of the different α values by investigating a two-parameter diagram for ϕ and α, concentrating especially on the creation of isolated limit cycles, which sometimes lead to further bifurcations inside the isola region. Figure 3 gives a two-parameter bifurcation diagram where ϕ and α are the free parameters. For low ϕ-values there is the Hopf bifurcation H and all other curves are tangent bifurcation curves.

Isolas appear or disappear upon crossing an isola variety. At an elliptic isola point an isolated solution branch is born, while at a hyperbolic isola point an isolated solution branch vanishes by coalescence with another branch [11]. From Figure 3 we see that at two values of $\alpha > 3$ isolas are born. Furthermore, period doubling bifurcations appear for lower α values, indicating the

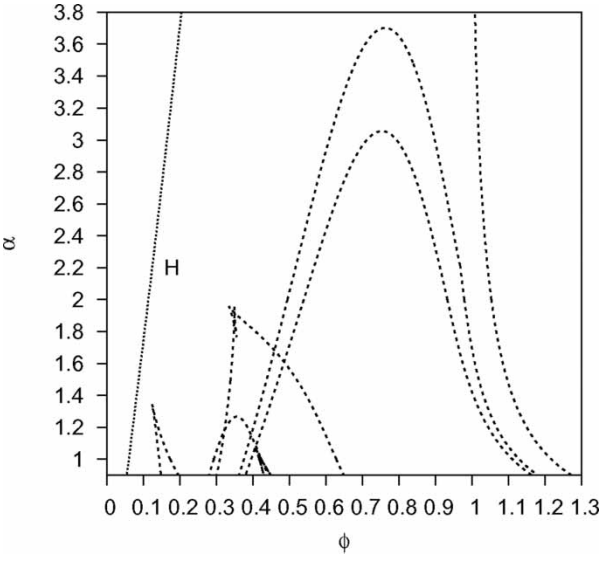

Figure 3. Two-dimensional parameter bifurcation diagram with ϕ and α as parameters. Only one Hopf bifurcation (dotted line) and many tangent bifurcation curves for limit cycles (dashed lines) are shown in the range $\alpha \in [1, 3.8]$. The isolated limit cycles originate above $\alpha = 3$. For lower values of α periodic doubling routes to chaos originate.

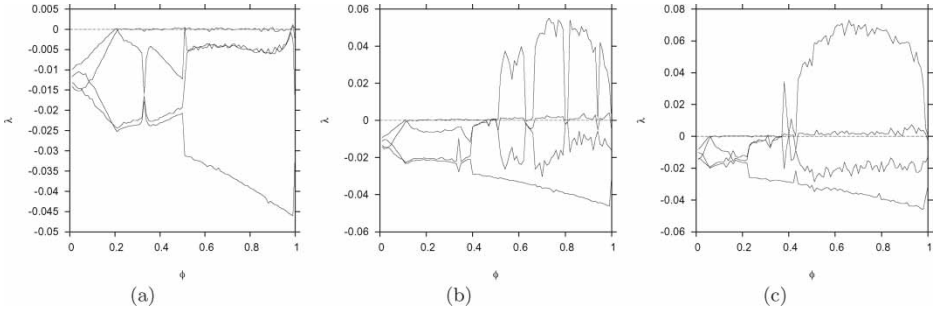

Figure 4. Spectrum of the four largest Lyapunov exponents with changing parameter ϕ and α fixed to the following values: (a) $\alpha = 4$, (b) $\alpha = 2$ and (c) $\alpha = 1$.

Feigenbaum route to chaos. However, only the calculation of Lyapunov exponents, which are discussed in the next section, can clearly indicate chaos.

5. Lyapunov spectra for various α values

The Lyapunov exponents are the logarithms of the eigenvalues of the Jacobian matrix along the integrated trajectories, Equation (2), in the limit of large integration times. With the exception of very simple iterated maps no analytic expressions for chaotic systems exists for the Lyapunov exponents. For the calculation of the iterated Jacobian matrix and its eigenvalues, we use the QR decomposition algorithm [9,19].

In Figure 4 we show the four largest Lyapunov exponents in the ϕ range between zero and one for various α values. For $\alpha = 4$ in Figure 4(a) we see for small ϕ values a fixed point behaviour indicated by a negative largest Lyapunov exponent up to around $\phi = 0.2$. There, at the Hopf bifurcation point, the largest Lyapunov exponent becomes zero, indicating limit cycle behaviour for the whole range of ϕ, apart from the final bit before $\phi = 1$, where a small spike with positive Lyapunov exponent might be present, but difficult to distinguish from the noisy numerical background.

For $\alpha = 2$ in Figure 4(b) however, we see a large window with positive largest Lyapunov exponent, well separated from the second largest one being zero. This is a clear sign of deterministically chaotic attractors being present for this ϕ range. Just a few windows with periodic attractors, indicated by the zero, largest Lyapunov exponents are visible in the region of $0.5 < \phi < 1$. For smaller ϕ values we observe qualitatively the same behaviour as already seen for $\alpha = 4$. For the smaller value of $\alpha = 1$ in Figure 4(c) the chaotic window is even larger than for $\alpha = 2$. Hence deterministic chaos is present for temporary cross immunity in the range around $\alpha = 2\,\text{year}^{-1}$ and for ϕ between zero and one.

6. Conclusions

We have presented a detailed bifurcation analysis for a multi-strain dengue fever model in terms of the ADE parameter ϕ, in the previously not very well-investigated region between zero and one, and a parameter for the temporary cross immunity α. The symmetries implied by the strain structure are taken into account in the analysis. Many of the possible bifurcations of equilibria and limit cycles of $\mathbb{Z}_2$-equivariant systems can be distinguished. Using AUTO [7] the different dynamical structures were calculated and coexisting attractors detected. In stochastic versions of the present

model [1] such coexisting attractors and eventually even transient chaos can be visited by the same system, leading to rather a more complicated dynamical behaviour than simpler one [8].

Future time series analysis of epidemiological data has good chances to give insight into the relevant parameter values purely on topological information of the dynamics, rather than by using the classical parameter estimation of which application is in general restricted to fairly simple dynamical scenarios.

Acknowledgements

This work has been supported by the European Union under the Marie Curie grant MEXT-CT-2004-14338. We thank Gabriela Gomes and Luis Sanchez, Lisbon, for scientific support.

Note

1. Equilibria are often called fixed points in dynamical systems theory; here we try to avoid this term, since in symmetry the term *fixed* is used in a more specific way.

References

[1] M. Aguiar and N. Stollenwerk, *A new chaotic attractor in a basic multi-strain epidemiological model with temporary cross-immunity* arXiv:0704.3174v1 [nlin.CD] (2007). Available at http://arxive.org.
[2] M. Aguiar, B.W. Kooi, and N. Stollenwerk, *Epidemiology of dengue fever: A model with temporary cross-immunity and possible secondary infection shows bifurcations and chaotic behaviour in wide parameter regions*, Math. Model. Nat. Phenom. 3 (2008), pp. 48–70.
[3] D. Albers and J. Sprott, *Routes to chaos in high-dimensional dynamical systems: a qualitative numerical study*, Physica D 223 (2006), pp. 194–207.
[4] L. Billings, B.I. Schwartz, B.L. Shaw, M. McCrary, D.S. Burke, and T.A.D. Cummings, *Instabilities in multiserotype disease models with antibody-dependent enhancement*, J. Theoret. Biol. 246 (2007), pp. 18–27.
[5] M.P. Boer, B.W. Kooi, and S.A.L.M. Kooijman, *Homoclinic and heteroclinic orbits in a tri-trophic food chain*, J. Math. Biol. 39 (1999), pp. 19–38.
[6] M.P. Boer, B.W. Kooi, and S.A.L.M. Kooijman, *Multiple attractors and boundary crises in a tri-trophic food chain*, Math. Biosci. 169 (2001), pp. 109–128.
[7] E.J. Doedel, R.C. Paffenroth, A.R. Champneys, T.F. Fairgrieve, Y.A. Kusnetsov, B. Sandstede, B. Oldeman, X.J. Wang, and C. Zhang, *AUTO 07P – Continuation and bifurcation software for ordinary differential equations*, Tech. Rep.: Concordia University, Montreal, Canada (2007). Available at http://indy.cs.concordia.ca/auto/
[8] F.R. Drepper, R. Engbert, and N. Stollenwerk, *Nonlinear time series analysis of empirical population dynamics*, Ecol. Modelling 75/76 (1994), pp. 171–181.
[9] J.P. Eckmann, S. Oliffson-Kamphorst, D. Ruelle, and S. Ciliberto, *Liapunov exponents from time series*, Phys. Rev. A 34 (1986), pp. 4971–4979.
[10] N. Ferguson, R. Anderson, and S. Gupta, *The effect of antibody-dependent enhancement on the transmission dynamics and persistence of multiple-strain pathogens*, Proc. Natl. Acad. Sci. USA 96 (1999), pp. 790–794.
[11] M. Golubitsky and D.G. Schaeffer, *Singularities and Groups in Bifurcation Theory*, Springer, New York, 1985.
[12] S.B. Halstead, *Neutralization and antibody-dependent enhancement of dengue viruses*, Adv. Virus Res. 60 (2003), pp. 421–467.
[13] B.W. Kooi and M.P. Boer, *Chaotic behaviour of a predator-prey system*, Dyn. Contin. Discrete Impuls. Syst., Ser. B: Appl. Algorithms 10 (2003), pp. 259–272.
[14] B.W. Kooi, L.D.J. Kuijper, and S.A.L.M. Kooijman, *Consequence of symbiosis for food web dynamics*, J. Math. Biol. 49 (2004), pp. 227–271.
[15] Y.A. Kuznetsov, *Elements of Applied Bifurcation Theory*, Applied Mathematical Sciences, vol. 112, 3rd ed., Springer-Verlag, New York, 2004.
[16] E. Massad, M. Chen, S. Ma, C.J. Struchiner, N. Stollenwerk, and M. Aguiar, *Scale-free network for a dengue epidemic*, Appl. Math. Comput. 159 (2008), pp. 376–381.
[17] Y. Nagao and K. Koelle, *Decreases in dengue transmission may act to increase the incidence of dengue hemorrhagic fever*, Proc. Natl. Acad. Sci. USA 105 (2008), pp. 2238–2243.
[18] E. Ott, *Chaos in Dynamical Systems*, Cambridge University Press, Cambridge, 2002.
[19] U. Parlitz, *Identification of true and spurious Lyapunov exponents from time series*, Int. J. Bifur. Chaos 2 (1992), pp. 155–165.
[20] D. Ruelle, *Chaotic Evolution and Strange Attractors*, Cambridge University Press, Cambridge, 1989.

[21] N. Stollenwerk and V.A.A. Jansen, *Evolution towards criticality in an epidemiological model for meningococcal disease*, Phys. Lett. A 317 (2003), pp. 87–96.
[22] N. Stollenwerk, M.C.J. Maiden, and V.A.A. Jansen, *Diversity in pathogenicity can cause outbreaks of menigococcal disease*, Proc. Natl. Acad. Sci. USA 101 (2004), pp. 10229–10234.
[23] R. Seydel, *Practical Bifurcation and Stability Analysis-from Equilibrium to Chaos*, Springer-Verlag, New York, 1994.
[24] H.J. Wearing and P. Rohani, *Ecological and immunological determinants of dengue epidemics*, Proc. Natl. Acad. Sci. USA 103 (2006), pp. 11802–11807.

Appendix A. Epidemic model equations

The complete system of ODEs for a two strain epidemiological system allowing for differences in primary versus secondary infection and temporary cross immunity is given by

$$\begin{aligned}
\frac{\mathrm{d}}{\mathrm{d}t}S &= -\frac{\beta}{N}S(I_1+\phi I_{21}) - \frac{\beta}{N}S(I_2+\phi I_{12}) + \mu(N-S),\\
\frac{\mathrm{d}}{\mathrm{d}t}I_1 &= \frac{\beta}{N}S(I_1+\phi I_{21}) - (\gamma+\mu)I_1,\\
\frac{\mathrm{d}}{\mathrm{d}t}I_2 &= \frac{\beta}{N}S(I_2+\phi I_{12}) - (\gamma+\mu)I_2,\\
\frac{\mathrm{d}}{\mathrm{d}t}R_1 &= \gamma I_1 - (\alpha+\mu)R_1,\\
\frac{\mathrm{d}}{\mathrm{d}t}R_2 &= \gamma I_2 - (\alpha+\mu)R_2,\\
\frac{\mathrm{d}}{\mathrm{d}t}S_1 &= -\frac{\beta}{N}S_1(I_2+\phi I_{12}) + \alpha R_1 - \mu S_1,\\
\frac{\mathrm{d}}{\mathrm{d}t}S_2 &= -\frac{\beta}{N}S_2(I_1+\phi I_{21}) + \alpha R_2 - \mu S_2,\\
\frac{\mathrm{d}}{\mathrm{d}t}I_{12} &= \frac{\beta}{N}S_1(I_2+\phi I_{12}) - (\gamma+\mu)I_{12},\\
\frac{\mathrm{d}}{\mathrm{d}t}I_{21} &= \frac{\beta}{N}S_2(I_1+\phi I_{21}) - (\gamma+\mu)I_{21},\\
\frac{\mathrm{d}}{\mathrm{d}t}R &= \gamma(I_{12}+I_{21}) - \mu R.
\end{aligned} \tag{A.1}$$

For two different strains, 1 and 2, we label the SIR classes for the hosts that have seen the individual strains. Susceptibles to both strains (S) get infected with strain 1 (I_1) or strain 2 (I_2), with infection rate β. They recover from infection with strain 1 (becoming temporary cross-immune R_1) or from strain 2 (becoming R_2), with recovery rate γ, and so on. With rate α, the R_1 and R_2 enter again in the susceptible classes (S_1 being immune against strain 1 but susceptible to 2, respectively, S_2), where the index represents the first infection strain. Now, S_1 can be reinfected with strain 2 (becoming I_{12}), meeting I_2 with infection rate β or meeting I_{12} with infection rate $\phi\beta$, secondary infected contributing differently to the force of infection than primary infected, and so on.

We include demography of the host population denoting the birth and death rate by μ. For constant population size N we have for the immune to all strains $R = N - (S + I_1 + I_2 + R_1 + R_2 + S_1 + S_2 + I_{12} + I_{21})$ and therefore we only need to consider the first nine equations of Equation (A.1), giving nine Lyapunov exponents. In our numerical studies we take the population size $N = 100$ so that mean proportions of susceptibles, infected, etc. are given in percentage. As fixed parameter values we take $\mu = (\frac{1}{65})\,\mathrm{year}^{-1}$, $\gamma = 52\,\mathrm{year}^{-1}$, $\beta = 2\cdot\gamma$. The parameters ϕ and α are varied.